

Interventional and Counterfactual Inference with Diffusion Models

Patrick Chao * Patrick Blöbaum
University of Pennsylvania Amazon
pchao@wharton.upenn.edu bloebp@amazon.com

Shiva Prasad Kasiviswanathan
Amazon
kasivisw@gmail.com

Abstract

We consider the problem of answering observational, interventional, and counterfactual queries in a causally sufficient setting where only observational data and the causal graph are available. Utilizing the recent developments in diffusion models, we introduce diffusion-based causal models (DCM) to learn causal mechanisms, that generate unique latent encodings to allow for direct sampling under interventions as well as abduction for counterfactuals. We utilize DCM to model structural equations, seeing that diffusion models serve as a natural candidate here since they encode each node to a latent representation, a proxy for the exogenous noise, and offer flexible and accurate modeling to provide reliable causal statements and estimates. Our empirical evaluations demonstrate significant improvements over existing state-of-the-art methods for answering causal queries. Our theoretical results provide a methodology for analyzing the counterfactual error for general encoder/decoder models which could be of independent interest.

1 Introduction

Understanding the causal relationships in complex problems is crucial for making analyses, conclusions, and generalized predictions. To do so, causal models and queries are necessary. Structural equation models (SEMs) are generative models describing the causal relationships between variables, allowing for observational, interventional, and counterfactual queries [Pearl, 2009]. SEMs are comprised of the underlying causal graph and structural equations that exactly dictate how variables affect one another. The causal graph in this work is assumed to be a directed acyclic graph (DAG) and given as prior knowledge. If the graph is not known, *causal discovery* algorithms can, under strong assumptions, be used instead to infer them from the data [Spirtes et al., 2000, Peters et al., 2017].

In this work, we assume causal sufficiency (i.e., absence of hidden confounders) and focus on approximating the structural equations given observational data and the underlying causal DAG, and providing a mechanism for answering all the three types of causal (observational, interventional, and counterfactual) queries [Pearl, 2009].

Based on Pearl’s graphical causal model framework, causal queries can be answered by learning a proxy for the unobserved exogenous noise and the structural equations. This suggests that learning *latent variable models* or *autoencoders* could be an attractive choice for the modeling procedure as the latent serves as the proxy for the exogenous noise. In autoencoders, the encoding process extracts the latent from an observation, and the decoding process generates the sample from the latent, approximating the SEM.

Recently, diffusion models [Sohl-Dickstein et al., 2015, Ho et al., 2020, Song et al., 2021] have become popular due to their expressivity and state-of-the-art performance for generative tasks with successful applications in image, text-to-image, image-to-image, audio generation, etc. [Saharia et al., 2022, Ramesh et al., 2022, Kong et al., 2021].

In this work, we propose and analyze the effectiveness of using a diffusion model for causal queries. Our main idea is to model each non-root node in the causal graph as a small diffusion model and cascade generated samples

*Work done during internship at Amazon.

in topological order. For each node, the corresponding diffusion model takes as input the node and parent values to encode and decode a latent representation. For the diffusion side, we utilize the recently proposed *Denoising Diffusion Implicit Models* (DDIMs) [Song et al., 2021], which may be interpreted as a deterministic autoencoder model with latent variables. We refer to the resulting model as *diffusion-based causal model* (DCM) and show that this model mimics the necessary properties of a causal model with unknown SEMs. Our key contributions include:

- (1) [Section 3] We propose diffusion-based causal model (DCM) as a flexible and practical framework for approximating both interventions (do-operator) and counterfactuals (abduction-action-prediction steps). We present a procedure for training a DCM given just the causal graph and observational data, and show that the resulting trained model enables sampling from the observational and interventional distributions, and answering counterfactual queries.
- (2) [Section 4] We theoretically analyze the counterfactual error provided by DCM and show that under some reasonable assumptions, it can be bounded. In fact, our analyses are quite general and hold beyond diffusion models to other encoder-decoder settings too. These bounds could be viewed as a first step towards explaining the performance gains that we observe in using deep generative models such as diffusion models for answering causal queries.
- (3) [Section 5] We evaluate the performance of DCM on a range of synthetic datasets generated with various structural equation types for all three forms of causal queries, namely evaluating the maximum mean discrepancy (MMD) for the generated and true observational and interventional distribution and the mean squared error (MSE) for counterfactual queries. We find that DCM consistently outperforms existing state-of-the-art methods [Sánchez-Martín et al., 2021, Khemakhem et al., 2021]. In fact, for certain interventional and counterfactual queries such as those arising with *nonadditive noise* models, DCM is better by an order of magnitude or more than these existing approaches. Finally, we show that our method also performs favorably for an interventional query experiment on fMRI data.

1.1 Related Work

Over the years, a variety of methods have been developed in the causal inference literature for answering interventional and/or counterfactual queries including non-parametric methods [Shalit et al., 2017, Alaa and Van Der Schaar, 2017, Muandet et al., 2021] and probabilistic modeling methods [Zečević et al., 2021]. More relevant to our approach is a recent series of work including Moraffah et al. [2020], Pawlowski et al. [2020], Kocaoglu et al. [2018], Parafita and Vitrià [2020], Garrido et al. [2021], Karimi et al. [2020], Sánchez-Martín et al. [2021], Khemakhem et al. [2021], Sanchez and Tsafaris [2022] that have demonstrated the success of using deep generative models for this task.

For example, Karimi et al. [2020] propose an approach for answering interventional queries by fitting a *conditional variational autoencoder* to each conditional in the Markov factorization implied by the causal graph. Also using the ideas of variational inference and normalizing flows Pawlowski et al. [2020] propose schemes that also allow for counterfactual inference.

In Khemakhem et al. [2021], the authors propose an autoregressive normalizing flow for causal discovery and queries, referred to as *CAREFL*. While the authors focus on bivariate graphs between observed and unobserved variables, their approach can be extended to more general DAGs. However, as also noted by Sánchez-Martín et al. [2021], CAREFL is unable to exploit the absence of edges fully as it reduces a causal graph to its causal ordering (which may not be unique). Sánchez-Martín et al. [2021] propose *VACA*, which uses graph neural networks (GNNs) in the form of a *variational graph autoencoder* to sample from the observational, interventional, and counterfactual distribution. VACA can utilize the inherent graph structure through the GNN, however, suffers in empirical performance (see Section 5). Furthermore, the usage of the GNN leads to undesirable design constraints, e.g., the encoder GNN cannot have hidden layers.

Sanchez and Tsafaris [2022] also uses diffusion models for counterfactual estimation, focusing on the bivariate graph case with an image class causing an image. The authors train a diffusion model to generate images and use the abduction-action-prediction procedure from Pearl et al. [2016] as well as classifier guidance [Dhariwal and Nichol, 2021] to generate counterfactual images. However, this is solely for bivariate models and requires training a separate classifier for intermediate diffusion images, and exhibits poor performance for more complex images

e.g., ImageNet [Deng et al., 2009]. We generalize their approach to arbitrary causal graphs, utilize classifier-free guidance [Ho and Salimans, 2021], and additionally address observational and interventional queries.

2 Preliminaries

Notation. To distinguish random variables from their instantiation, we represent the former with capital letters and the latter with the corresponding lowercase letters. To distinguish between the nodes in the causal graph and diffusion random variables, we use subscripts to denote graph nodes and superscripts to denote the time index in the diffusion process, and let $[n] = \{1, \dots, n\}$ for $n \in \mathbb{Z}^+$.

Structural Causal Models (SCMs). Consider a directed acyclic graph (DAG) \mathcal{G} with nodes $\mathcal{V} = \{1, \dots, K\}$ and edges \mathcal{E} , where node i is represented by a (random) variable X_i in some generic space \mathcal{X}_i . Let pa_i be the parents of node i in \mathcal{G} and let $X_{\text{pa}_i} := \{X_j\}_{j \in \text{pa}_i}$ be the variables of the parents of node i . Without loss of generalization, assume the nodes \mathcal{V} are in topologically sorted order. A structural causal model (SCM) \mathcal{M} describes the relationship between a observed/endogenous node i and its causal parents, \mathcal{M} is comprised of structural equations $f = (f_1, \dots, f_K)$ and prior distributions $p(U_i)$ for unobserved/exogenous random variables (U_1, \dots, U_K) , where: $X_i = f_i(X_{\text{pa}_i}, U_i)$ for $i \in [K]$. Furthermore, the unobserved random variables are assumed to be jointly independent (i.e., assuming causal sufficiency), implying X_i is solely a function of its direct parents and its exogenous variable U_i , inducing an observation distribution: $p(X_1, \dots, X_K) = \prod_{i=1}^K p(X_i | X_{\text{pa}_i})$.

Structural causal models address Pearl’s causal hierarchy (or “ladder of causation”), three “layers” (or “rungs”) of causal queries in increasing difficulty [Pearl, 2009], associational, interventional, and counterfactual queries.

1. **Associational Queries:** Evaluate the observational distribution $p(X_1, \dots, X_K)$.
2. **Interventional Queries:** Evaluate the interventional distribution $p(X | \text{do}(X_{\mathcal{I}} := \gamma))$.
3. **Counterfactual Queries:** Given a factual sample X^{F} , evaluate the counterfactual distribution $p(X^{\text{CF}} | X^{\text{F}}, \text{do}(X_{\mathcal{I}} := \gamma))$.

For the rest of this paper, we use ‘observational queries’ to also represent ‘associational queries’, since they are sampling the observational distribution.

The do-operator $\text{do}(X_i := \gamma_i)$, here exemplary as an atomic intervention, represents the effect of setting variable X_i to γ_i . This may be interpreted as removing all incoming edges to node i and setting $X_i = \gamma_i$, therefore only affecting descendants of node i . Note that our proposed framework allows for more general sets of interventions as well, such as interventions on multiple variables denoted as $\text{do}(X_{\mathcal{I}} := \gamma)$ where a set of variables $\mathcal{I} \subset [K]$ are intervened with values γ_i respectively. Interventional queries address the distribution of X when a subset is set to γ , notably different than conditioning on $X_{\mathcal{I}} = \gamma$. Counterfactual queries address the distribution of X^{CF} for a fixed factual observation X^{F} when a subset is intervened to γ . Counterfactual estimation may be performed through the three-step procedure of 1) abduction: estimation of the exogenous noise U , 2) action: intervene $\text{do}(X_{\mathcal{I}} := \gamma)$, and 3) prediction: estimating X^{CF} using the abducted noise and intervention values.

Diffusion Models. The objective of diffusion models is given data from distribution $X^0 \sim Q$, learn an efficiently sampleable distribution close to Q . Denoising diffusion probabilistic models (DDPMs) [Sohl-Dickstein et al., 2015, Ho et al., 2020] accomplish this by introducing a forward noising process that adds isotropic Gaussian noise at each time step and a learned reverse denoising process.

A common representation of diffusion models is a fixed Markov chain that adds Gaussian noise with variances $\beta_1, \dots, \beta_T \in (0, 1)$, generating latent variables X^1, \dots, X^T ,

$$\begin{aligned} q(X^t | x^{t-1}) &= \mathcal{N}(X^t; \sqrt{1 - \beta_t}x^{t-1}, \beta_t I) \\ q(X^t | x^0) &= \mathcal{N}(X^t; \sqrt{\alpha_t}x^0, (1 - \alpha_t)I) \end{aligned}$$

where $\alpha_t = \prod_{i=1}^t (1 - \beta_i)$.

By choosing sufficiently large T and α_t that converge to 0, we have X^T is distributed as an isotropic Gaussian distribution. The learned reverse diffusion process attempts to approximate the intractable $q(X^{t-1} | x^t)$ using a neural network and is defined as a Markov chain with Gaussian transitions,

$$p_{\theta}(X^{t-1} | x^t) = \mathcal{N}(X^{t-1}; \mu_{\theta}(x^t, t), \Sigma_{\theta}(x^t, t)).$$

Rather than predicting μ_θ directly, the network could instead predict the noise ε from $x^t = \sqrt{\alpha_t}x^0 + \sqrt{1 - \alpha_t}\varepsilon$. Ho et al. [2020] found that modeling ε instead of μ_θ , fixing Σ_θ , and using the following reweighted loss function

$$\mathbb{E}_{\substack{t \sim \text{Unif}\{[T]\} \\ X^0 \sim Q \\ \varepsilon \sim \mathcal{N}(0, I)}} [\|\varepsilon - \varepsilon_\theta(\sqrt{\alpha_t}X^0 + \sqrt{1 - \alpha_t}\varepsilon, t)\|^2], \quad (1)$$

works well empirically. We also utilize this loss function in our training.

Song et al. [2021] introduce a richer family of distributions with parameters $\sigma \in \mathbb{R}_{\geq 0}^T$, where it is possible to use a pretrained DDPM model to obtain a deterministic sample given noise X^T , known as the denoising diffusion implicit model (DDIM), with *reverse implicit diffusion process*

$$X^{t-1} = \sqrt{\frac{\alpha_{t-1}}{\alpha_t}}X^t - \varepsilon_\theta(X^t, t) \cdot \left(\sqrt{\alpha_{t-1}(1 - \alpha_t)/\alpha_t} - \sqrt{1 - \alpha_{t-1}} \right). \quad (2)$$

We also use a *forward implicit diffusion process* introduced by Song et al. [2021], derived from rewriting the DDIM process (2) as an ordinary differential equation (ODE) and considering the Euler method approximation in the forward direction to obtain

$$X^{t+1} = \sqrt{\frac{\alpha_{t+1}}{\alpha_t}}X^t + \varepsilon_\theta(X^t, t) \cdot \left(\sqrt{1 - \alpha_{t+1}} - \sqrt{\alpha_{t+1}(1 - \alpha_t)/\alpha_t} \right). \quad (3)$$

3 Diffusion-based Causal Models

In this section, we present how denoising diffusion implicit models can be used for answering causal queries. We first explain the construction and the training process, and in Section 3.1, we explain how the model can be used for answering various causal queries.

Given causal graph \mathcal{G} over endogenous variables (X_1, \dots, X_K) , we may topologically sort the graph and relabel the nodes, implying $j < i$ for all $j \in \text{pa}_i$, and assume $X_i \in \mathbb{R}^{d_i}$. We start with some notations.

- Define Z_i^t to be the i th endogenous node value at diffusion step t of the forward implicit diffusion process, and let $Z_i := Z_i^T$.
- Define \hat{X}_i^t to be i th endogenous node value at diffusion step t of the reverse implicit diffusion process, and let $\hat{X}_i := \hat{X}_i^0$.

We train a diffusion model for *each node*, taking denoised parent values as input. The parent values can be interpreted as additional covariates to the model, where one may choose to use classifier free guidance to incorporate the covariates [Ho and Salimans, 2021]. Empirically, we find that simply concatenating the covariates results in better performance than classifier free guidance, and provide theoretical intuition for this phenomenon in Theorem 1 and Section 5.

We use the ε_θ parametrization for the diffusion model from Ho et al. [2020], representing the diffusion model for node i as $\varepsilon_\theta^i(X, X_{\text{pa}_i}, t)$. The complete training procedure presented in Algorithm 1 is only slightly modified from the usual training procedure, with the additions of the parents as covariates and training a diffusion model for each node. Notably, since these losses are independent for each node, each diffusion model may be trained in parallel.

Using the forward implicit diffusion process in Eq. (3), given a sample, we may encode a unique latent variable Z_i that acts as a proxy for the exogenous noise U_i . The latent variable Z_i is not necessarily equivalent to the exogenous U_i , which is not required, and instead represents the unexplained information of X_i from X_{pa_i} .

Using the reverse implicit diffusion process from DDIM in Eq. (2), given a latent vector Z (or by sampling $Z \sim \mathcal{N}(0, I)$) we may obtain a deterministic decoding \hat{X} . The decoding process is identical to the DDIM decoding process except we include the decoded parent values as covariates, and decode the graph in topological order.

Algorithm 1 DCM Training

Input: Distribution Q , scale factors $\{\alpha_t\}_{t=1}^T$, causal DAG \mathcal{G} with node i represented by X_i

```
1: while not converged do
2:   Sample  $X^0 \sim Q$ 
3:   for  $i = 1, \dots, K$  do
4:      $t \sim \text{Unif}[\{1, \dots, T\}]$ 
5:      $\varepsilon \sim \mathcal{N}(0, I)$ 
6:     Update parameters of node  $i$ 's diffusion model  $\varepsilon_\theta^i$ , by minimizing the following loss (based on (1)) :
7:      $\left\| \varepsilon - \varepsilon_\theta^i(\sqrt{\alpha_t}X_i^0 + \sqrt{1 - \alpha_t}\varepsilon, X_{\text{pa}_i}^0, t) \right\|_2^2$ 
8:   end for
9: end while
```

We define $\text{Enc}_i(X_i, X_{\text{pa}_i})$ and $\text{Dec}_i(Z_i, X_{\text{pa}_i})$ to be the implicit encoding and decoding functions for node i defined in Eqns. (3) and (2) respectively when applied recursively T times, explicitly defined in Algorithms 4 and 5 (presented in Appendix A) respectively.

3.1 Answering Causal Queries with DCM

For interventional and counterfactual queries, consider a set of intervention variables \mathcal{I} and values γ , where $\text{do}(\mathcal{I} := \gamma) := \{\text{do}(X_i := \gamma_i)\}_{i \in \mathcal{I}}$.

Observational/Interventional Queries. For an intervened node i with intervention γ_i , the sampled value is always the intervention value, therefore we generate $\hat{X}_i = \gamma_i$. For root nodes, we sample \hat{X}_i from the empirical distribution of the training set. For a non-intervened non-root node i , assume by induction we have the generated parent values \hat{X}_{pa_i} . To generate \hat{X}_i , we first sample the latent vector $Z_i \sim \mathcal{N}(0, I_{d_i})$ where d_i is the dimension of X_i . Then taking Z_i as the noise for node i , we compute $\hat{X}_i = \text{Dec}_i(Z_i, \hat{X}_{\text{pa}_i})$ as the generated sample value for node i . This value \hat{X}_i is then used as the parent value for the children of node i . For observational samples, we perform the same process but with $\mathcal{I} = \emptyset$. This is summarized in Algorithm 2.

Algorithm 2 Observational/Interventional Sampling

Input: Intervention set \mathcal{I} with values γ , optional noise $Z_i \sim \mathcal{N}(0, I_{d_i})$ for $i \in [K]$

```
1: for  $i = 1, \dots, K$  do
2:   if  $i \in \mathcal{I}$  then
3:      $\hat{X}_i = \gamma_i$ 
4:   else if  $i$  is a root node then
5:      $\hat{X}_i \sim E_i$ , the empirical distribution
6:   else
7:      $\hat{X}_i \leftarrow \text{Dec}_i(Z_i, \hat{X}_{\text{pa}_i})$ 
8:   end if
9: end for
10: Return  $\hat{X}$ 
```

Algorithm 3 Counterfactual Inference

Input: Intervention set \mathcal{I} with values γ , factual sample X^F

```
1: Abduction:  $Z_i^F \leftarrow \text{Enc}_i(X_i^F, X_{\text{pa}_i}^F)$  for  $i \in [K]$ 
2: Action and Prediction: Apply Algorithm 2 on  $Z^F, \mathcal{I}, \gamma$  to obtain  $\hat{X}^{\text{CF}}$ 
3: Return  $\hat{X}^{\text{CF}}$ 
```

Counterfactual Queries. For a factual observation X^F and interventions on nodes \mathcal{I} with values γ , let \hat{X}^{CF}

be the generated counterfactual value. The counterfactual estimate \hat{X}^{CF} only differs from the factual estimate X^{F} for all nodes that are intervened upon or downstream from an intervened node. Similarly to interventional queries, for each intervened node i , $\hat{X}_i^{\text{CF}} = \gamma_i$. For each non-intervened node i downstream from an intervened node, assume by induction that we have the generated counterfactual estimates $\hat{X}_{\text{pa}_i}^{\text{CF}}$. To obtain \hat{X}_i^{CF} , we first perform 1) *abduction*; define the estimated factual noise as $\hat{Z}_i^{\text{F}} = \text{Enc}_i(X_i^{\text{F}}, X_{\text{pa}_i}^{\text{F}})$. Then we may generate our counterfactual estimate from 2) *action* by using \hat{Z}_i^{F} as the noise for node i and 3) *prediction* by decoding, $\hat{X}_i^{\text{CF}} = \text{Dec}_i(\hat{Z}_i^{\text{F}}, \hat{X}_{\text{pa}_i}^{\text{CF}})$. This is summarized in Algorithm 3.

4 Bounding Counterfactual Error

We now establish conditions under which the counterfactual estimation error can be bounded. In fact, the results in this section not only hold for diffusion models, but to a more general setting of encoder-decoder models satisfying certain properties.

Consider a node i (represented by $X_i \in \mathcal{X}_i$) in the causal graph and its parents (represented by $X_{\text{pa}_i} \in \mathcal{X}_{\text{pa}_i}$). The following Theorem 1 bounds the counterfactual error in terms of the reconstruction error of the encoder-decoder network at node i . Informally, the theorem shows that for an encoding function $g : \mathcal{X}_i \times \mathcal{X}_{\text{pa}_i} \rightarrow \mathcal{Z}$ and decoding function $h : \mathcal{Z} \times \mathcal{X}_{\text{pa}_i} \rightarrow \mathcal{X}_i$, if the reconstruction $h(g(X_i, X_{\text{pa}_i}), X_{\text{pa}_i})$ is “close” to X_i (measured under some metric $d(\cdot, \cdot)$), then such encoder-decoder networks can provide “good” counterfactual estimates under some additional conditions. To the best of our knowledge this is the first result that bounds the counterfactual error in terms of the reconstruction error of these encoder-decoder networks. Since the choice of node i plays no role, we drop the subscript i in the following.

Theorem 1. *Assume for $X \in \mathcal{X} \subset \mathbb{R}$ and exogenous noise $U \sim \text{Unif}[0, 1]$, X satisfies the structural equation: $X = f(X_{\text{pa}}, U)$, where $X_{\text{pa}} \in \mathcal{X}_{\text{pa}} \subset \mathbb{R}^d$ are the parents of node X and $U \perp\!\!\!\perp X_{\text{pa}}$.*

Consider an encoder-decoder model with encoding function $g : \mathcal{X} \times \mathcal{X}_{\text{pa}} \rightarrow \mathcal{Z}$ and decoding function $h : \mathcal{Z} \times \mathcal{X}_{\text{pa}} \rightarrow \mathcal{X}$,

$$Z = g(X, X_{\text{pa}}), \quad \hat{X} = h(Z, X_{\text{pa}}).$$

Assume the following conditions are met:

1. *The encoding is independent from the parent values, $g(X, X_{\text{pa}}) \perp\!\!\!\perp X_{\text{pa}}$.*
2. *Under some metric d e.g., $\|\cdot\|_2$, the model has reconstruction error less than τ ,*

$$d(h(g(X, X_{\text{pa}}), X_{\text{pa}}), X) \leq \tau. \tag{4}$$

3. *The structural equation f is invertible, differentiable, and increasing with respect to U .*
4. *The encoding g is invertible and differentiable with respect to X .*

Then for a sample (x_{pa}, x, u) and intervention $\text{do}(X_{\text{pa}} := \gamma)$, the counterfactual estimate from the model of the true counterfactual $x^{\text{CF}} = f(\gamma, u)$ has estimation error at most τ : $d(h(g(x, x_{\text{pa}}), \gamma), x^{\text{CF}}) \leq \tau$.

Discussion on Theorem 1. The proof for Theorem 1 is in Appendix B. We make the following observations about this result.

(1) The first assumption suggests encouraging independence between the encoding and the parent values. One may measure the dependence between encodings and parent values on training or hold out data to verify the claim, for example through measuring the Hilbert-Schmidt independence criterion (HSIC) [Gretton et al., 2007]. The heuristic of minimizing the dependence between regressors and residuals has been explored [Mooij et al., 2009]; our theoretical results independently motivate this heuristic.

¹To encourage independence, one could also modify the original diffusion model training objective to add an HSIC regularization term. Our experiments did not show a clear benefit of using this modified objective, and we leave further investigation for future work.

(2) The third assumption is always satisfied under the additive noise model (i.e., $X = f'(X_{\text{pa}}) + U$) or post non-linear models [Zhang and Hyvarinen, 2012]. The generalizability of the noise U allows for common noise distributions such as additive Gaussian noise.

(3) From the third assumption that the structural equation $X = f(X_{\text{pa}}, U)$ is invertible with respect to U in Theorems 1 and 3, this suggests that our latent variable should be of equal dimension to the X we are modeling. While some autoencoder models decrease the latent dimension with respect to the input, diffusion models retain the same dimension between X and U making them amenable to the above analysis.

(4) This theorem assumes a one-dimensional exogenous noise U and variable $X \in \mathcal{X} \subset \mathbb{R}$. We provide a similar theorem for the multivariate case where $X \in \mathbb{R}^m$ for $m \geq 3$ in Theorem 3 in the Appendix with a stronger assumption on the Jacobian of f and g . We leave relaxing the assumptions on the Jacobian for future work. Note that the dimension d of X_{pa} plays no role.

(5) We may consider transforms of the uniform noise U to obtain other settings, for example additive Gaussian noise. The only assumptions on the noise are independence and the third assumption, stating f is invertible, differentiable, and increasing with respect to U . For a continuous random variable U' with invertible CDF F and the structural equation $f(\cdot, F(\cdot))$, we have $U' \stackrel{d}{=} F^{-1}(U)$ and the results similarly hold.

(6) Theorem 1 suggests that the reconstruction error can serve as an estimate for the counterfactual error. While the true value of τ is unknown, we may compute a lower bound by computing the reconstruction error over the dataset.

Finally, while these conditions are needed for our proof, in practice even under violations, our DCM approach provides good empirical performance with low counterfactual error, suggesting the possibility of further refinement of the theorem statement.

5 Experimental Evaluation

In this section, we evaluate the empirical performance of DCM for answering causal queries on both synthetic and real world data.

ε_θ **Model Implementation.** For our implementation of the ε_θ model in DCM, we use a simple fully connected neural network with three hidden layers of size [128, 256, 256]. We fit the model using Adam with a learning rate of 1e-4, batch size of 64, and train for 500 epochs.

For the diffusion model parameters, we use $T = 100$ total time steps with a linear β_t schedule interpolating between 1e-4 and 0.1, or $\beta_t = (0.1 - 1e-4) \frac{t-1}{T-1} + 10^{-4}$ for $t \in [T]$. To incorporate the parents' values and time step t , we simply concatenate the parent values and t/T as input to the ε_θ model. We found that using the popular cosine schedule [Nichol and Dhariwal, 2021] resulted in worse empirical performance, as well as using a positional encoding for the time t . We believe the drop in performance from the positional encoding is due to the low dimensionality of the problem since the dimension of the positional encoder would dominate the dimension of the other inputs.

We also evaluated using classifier-free guidance (CFG) [Ho and Salimans, 2021] to improve the reliance on the parent values, however, we found this also decreased performance. We provide a plausible explanation that can be explained through Theorem 1. With Theorem 1, we would like our encoding $g(Y, X)$ to be independent of X , however using a CFG encoding $(1 + w)g(Y, X) - wg(Y, 0)$ would only serve to increase the dependence of $g(Y, X)$ on X , which is counterproductive to our objective.

5.1 Synthetic Data Experiments

For generating quantitative results, we use synthetic experiments since we know the exact structural equations, and hence we have access to the ground-truth observational, interventional, and counterfactual distributions.

Following Sánchez-Martín et al. [2021], for the observational and interventional distributions, we report the Maximum Mean Discrepancy (MMD) [Gretton et al., 2012] between the true and estimated distributions. For counterfactual estimation, we report the mean squared error (MSE) of the true and estimated counterfactual values.

We compare DCM to two recently proposed state-of-the-art schemes VACA [Sánchez-Martín et al., 2021] and CAREFL [Khemakhem et al., 2021], and a general regression model that assumes an additive noise model which we refer to as ANM. The ANM approach performs model selection over a variety of models, including linear

and gradient boosted regressor and we use the implementation from the popular *DoWhy* causal inference package [Sharma et al., 2019, Blöbaum et al., 2022]. Additional details on how ANM answers causal queries are provided in Appendix C.1 and implementation details for VACA, CAREFL, and ANM are in Appendix C.3.

We consider four graph structures, which we call the *chain*, *triangle*, *diamond*, and *Y* graphs (see Figure 2). Also as in Sánchez-Martín et al. [2021], we consider two broad classes of structural equations:

- Additive Noise Model (ANM): $f_i(X_{\text{pa}_i}, U_i) = f'(X_{\text{pa}_i}) + U_i$. In particular, we will be interested in the case where f_i 's are non-linear, referred henceforth as NLIN.
- Nonadditive Noise Model: $f_i(X_{\text{pa}_i}, U_i)$ is an arbitrary function of X_{pa_i} and U_i , referred henceforth as NADD.

The exact equations are presented in Table 3 (Appendix C) and discussed in Appendix C.2. These functional equations were chosen to balance the signal-to-noise ratio of the covariates and noise to represent realistic settings. Furthermore, these structural equations were chosen *after* hyperparameter selection, meaning we did not tune DCM's parameters nor tune the structural equations after observing the performance of the models.

Each simulation generates $n = 5000$ samples as training data. Let \hat{M} be a fitted causal model and M^* be the true causal model, both capable of generating observational and interventional samples, and answering counterfactual queries. Each pair of graph and structural equation type is evaluated for 10 different initialization and we report the mean value.

Observational Evaluation. We generate 1000 samples from both the fitted and true observational distribution and report the MMD between the two. Since DCM and the ANM use the empirical distribution for root nodes, we only take the MMD between nonroot nodes.

Interventional Evaluation. We consider interventions of individual nodes. For node i , We choose 20 intervention values $\gamma_1, \dots, \gamma_{20}$, linearly interpolating between the 10% and 90% quantiles of the marginal distribution of node i to represent realistic interventions. Then for each intervention $\text{do}(X_i := \gamma_j)$, we generate 100 values from the fitted model and true causal model, \hat{X} and X^* for the samples from the fitted model and true model respectively. Since the intervention only affects the descendants of node i , we subset \hat{X} and X^* to include only the descendants of node i , and compute the MMD on \hat{X} and X^* to obtain a distance $\delta_{i,j}$ between the interventional distribution for the specific node and interventional value. Lastly, we report the mean MMD over all 20 intervention values and all intervened nodes.

- 1: **for** each non-sink node i in graph **do**
- 2: $\gamma_1, \dots, \gamma_{20}$ linearly interpolate 10% to 90% quantiles of node i
- 3: **for** Intervention γ_j **do**
- 4: Intervene $\text{do}(X_i := \gamma_j)$
- 5: Generate 100 samples \hat{X} from \hat{M} and X^* from M^* of descendants of i
- 6: $\delta_{i,j} \leftarrow \text{MMD}(\hat{X}, X^*)$
- 7: **end for**
- 8: **end for**
- 9: Output mean of all $\delta_{i,j}$

Counterfactual Evaluation. Similarly to interventional evaluation, we consider interventions of individual nodes and for node i , we choose 20 intervention values $\gamma_1, \dots, \gamma_{20}$, linearly interpolating between the 10% and 90% quantiles of the marginal distribution of node i to represent realistic interventions. Then for each intervention $\text{do}(X_i := \gamma_j)$, we generate 100 nonintervened factual samples X^F , and query for the estimated and true counterfactual values \hat{X}^{CF} and $X^{\text{CF},*}$ respectively. Similarly to before, \hat{X}^{CF} and $X^{\text{CF},*}$ only differ on the descendants of node i , therefore we only consider the subset of the descendants of node i . We compute the MSE $\delta_{i,j}$, since the counterfactual estimate and ground truth are point values, giving us an error for a specific node and interventional value. Lastly, we report the mean MSE over all 20 intervention values and all intervened nodes.

- 1: **for** each non-sink node i in graph **do**
- 2: $\gamma_1, \dots, \gamma_{20}$ linearly interpolate 10% to 90% quantiles of node i
- 3: **for** Intervention γ_j **do**
- 4: Generate 100 factual samples X_1^F, \dots, X_{100}^F

- 5: Intervene $\text{do}(X_i := \gamma_j)$
- 6: Compute counterfactual estimates $\{\hat{X}_k^{\text{CF}}\}_{k=1}^{100}$ and $\{X_k^{\text{CF},*}\}_{k=1}^{100}$ from X^{F} of descendants of i
- 7: $\delta_{i,j} \leftarrow \text{MSE}(\{\hat{X}_k^{\text{CF}}\}_{k=1}^{100}, \{X_k^{\text{CF},*}\}_{k=1}^{100})$
- 8: **end for**
- 9: **end for**
- 10: Output mean of all $\delta_{i,j}$

Our Results. In Table 1, we provide the performance of all evaluated models for observational, interventional, and counterfactual queries, averaged over 10 separate initializations of models and training data, with the lowest value in each row bolded. The values are multiplied by 100 for clarity. In Figure 1 (Appendix C), we show the box plots for the same set of experiments.

Table 1: Mean \pm standard deviation of observational, interventional, and counterfactual queries of four different SCMs in nonlinear and nonadditive settings over 10 random initializations of the model and training data. The values are multiplied by 100 for clarity.

SCM	Metric	DCM	ANM	VACA	CAREFL	
		($\times 10^{-2}$)	($\times 10^{-2}$)	($\times 10^{-2}$)	($\times 10^{-2}$)	
<i>Triangle</i>	NLIN	Obs. MMD	0.10\pm0.04	0.14 \pm 0.08	2.36 \pm 0.64	4.80 \pm 0.60
		Int. MMD	1.41\pm0.33	4.88 \pm 0.97	18.55 \pm 1.42	9.32 \pm 0.86
		CF. MSE	2.24\pm0.62	17.73 \pm 3.77	294.78 \pm 35.27	24.51 \pm 8.37
	NADD	Obs. MMD	0.18\pm0.07	0.51 \pm 0.11	1.90 \pm 0.35	5.17 \pm 0.82
		Int. MMD	1.09\pm0.19	2.96 \pm 0.36	5.71 \pm 1.07	3.58 \pm 0.37
		CF. MSE	26.22\pm12.03	160.66 \pm 26.32	283.52 \pm 29.18	204.26 \pm 33.72
<i>Chain</i>	NLIN	Obs. MMD	0.25 \pm 0.09	0.14\pm0.08	1.65 \pm 0.46	4.47 \pm 0.92
		Int. MMD	1.43 \pm 0.34	1.38\pm0.37	9.71 \pm 2.01	13.43 \pm 0.92
		CF. MSE	0.32\pm0.21	1.94 \pm 3.61	33.22 \pm 8.93	15.04 \pm 7.72
	NADD	Obs. MMD	0.31\pm0.22	0.83 \pm 0.28	1.24 \pm 0.49	3.46 \pm 0.89
		Int. MMD	3.50\pm0.81	10.44 \pm 0.64	19.51 \pm 4.83	20.28 \pm 3.05
		CF. MSE	0.63\pm0.22	16.19 \pm 1.19	24.88 \pm 5.97	46.02 \pm 12.31
<i>Y</i>	NLIN	Obs. MMD	0.18 \pm 0.11	0.11\pm0.04	1.94 \pm 0.42	6.61 \pm 0.78
		Int. MMD	1.40\pm0.28	1.86 \pm 0.30	13.63 \pm 3.08	33.03 \pm 3.87
		CF. MSE	0.29\pm0.10	0.68 \pm 0.09	28.42 \pm 13.49	45.25 \pm 5.50
	NADD	Obs. MMD	0.26\pm0.09	0.97 \pm 0.21	1.35 \pm 0.35	3.29 \pm 0.46
		Int. MMD	1.75\pm0.27	11.28 \pm 0.98	8.47 \pm 1.22	11.08 \pm 1.11
		CF. MSE	77.89\pm4.13	99.98 \pm 4.76	131.30 \pm 5.86	100.35 \pm 10.51
<i>Diamond</i>	NLIN	Obs. MMD	0.29 \pm 0.14	0.13\pm0.04	2.52 \pm 0.14	8.25 \pm 1.00
		Int. MMD	7.75 \pm 1.90	3.38\pm0.90	45.23 \pm 1.77	16.04 \pm 4.35
		CF. MSE	40.99 \pm 10.27	11.44\pm2.29	289.13 \pm 10.94	43.23 \pm 16.27
	NADD	Obs. MMD	0.27\pm0.07	0.28 \pm 0.12	2.46 \pm 0.68	5.53 \pm 0.79
		Int. MMD	1.71\pm0.37	3.42 \pm 0.52	5.49 \pm 1.31	21.93 \pm 2.75
		CF. MSE	0.47\pm0.05	2.44 \pm 0.20	9.78 \pm 4.00	24.74 \pm 9.82

We see DCM and ANM are the most competitive approaches, with similar performance in the nonlinear settings where the ANM is correctly specified. These two approaches are comparable and outperform VACA and CAREFL by about an order of magnitude. DCM has the lowest error in 6 out of 12 of the nonlinear settings, with the correctly specified ANM having the lowest error in the remaining 6. Furthermore, DCM and ANM both typically have a lower standard deviation compared to the other competing methods.

For the nonadditive settings, DCM demonstrates the lowest values for all 12 causal queries. Notably, for the challenging task of counterfactual estimation, the improvement is quite large (one or even two orders of magnitude). Lastly, the standard deviation of DCM is small relative to the other models, demonstrating relative consistency which points to the robustness of our proposed approach.

5.2 Real Data Experiments

We evaluate DCM on interventional real world data by evaluating our model on the electrical stimulation interventional fMRI data from [Thompson et al., 2020], using the experimental setup from [Khemakhem et al., 2021]. The fMRI data comprises of samples from 14 patients with medically refractory epilepsy, with time series of the Cingulate Gyrus (CG) and Heschl’s Gyrus (HG). The assumed underlying causal structure is the bivariate graph $CG \rightarrow HG$. Our interventional ground truth data is comprised of an intervened value of CG and an observed sample of HG. We evaluate the median absolute error between the observed value of HG and the model’s predicted value. We defer the reader to [Thompson et al., 2020, Khemakhem et al., 2021] for a more thorough discussion of the dataset. Since we perform a pointwise comparison, for DCM we output the median sampled value of HG from 1000 generated samples. [Khemakhem et al., 2021] evaluate CAREFL, an additive noise model implemented from [Hoyer et al., 2008], and a linear SEM which performs a ridge regression. In Table 2, we see that DCM outperforms the other causal models.

Algorithm	Median Abs. Error
DCM	0.577
CAREFL	0.586
ANM	0.655
Linear SEM	0.643

Table 2: Median absolute error for interventional predictions on the fMRI data. The last three entries are from Table 2 in Khemakhem et al. [2021]. We do not include VACA due to implementation difficulties.

We note that the difference in performance is much more minor than our synthetic results. We believe this is due to two reasons. First, the data seems inherently close to linear, as exhibited by the relatively similar performance with the a standard ridge regression model. Second, to be consistent with the setup in Khemakhem et al. [2021], rather than evaluating the MMD of the true and predicted interventional distribution, we are reporting the median absolute error of a single observation. This introduces a possibly large amount of irreducible error, therefore artificially inflating the error values.

6 Discussion and Future Work

We demonstrate that diffusion models, in particular, the DDIM formulation (which allows for unique encoding and decoding) provide a flexible and practical framework for approximating interventions (do-operator) and counterfactual (abduction-action-prediction) steps. Our approach, DCM, is applicable independent of the DAG structure and makes no assumptions on the structural equations. We find that empirically DCM outperforms competing methods in all three causal settings, observational, interventional, and counterfactual queries, across various classes of structural equations and graphs.

One potential avenue for improvement would be to encourage independence between the encoding and parent values, as suggested by Theorem 1.

Additionally on the practical side, we may generalize our approach to high-dimensional settings such as images. Another potential idea is to combine our techniques with the recent result of Saha and Garain who demonstrated that it may not be necessary to abduct all the noise variables in a structural causal model (SCM) to answer a counterfactual query.

Acknowledgements

We would like to thank Dominik Janzing, Lenon Minorics and Atalanti Mastakouri for helpful discussions surrounding this project.

References

- Ahmed M Alaa and Mihaela Van Der Schaar. Bayesian inference of individualized treatment effects using multi-task gaussian processes. *Advances in neural information processing systems*, 30, 2017.
- David E Blair. *Inversion theory and conformal mapping*, volume 9. American Mathematical Soc., 2000.
- Patrick Blöbaum, Peter Götz, Kailash Budhathoki, Atalanti A. Mastakouri, and Dominik Janzing. Dowhy-gcm: An extension of dowhy for causal inference in graphical causal models. *arXiv preprint arXiv:2206.06821*, 2022.
- Jia Deng, Wei Dong, Richard Socher, Li-Jia Li, Kai Li, and Li Fei-Fei. Imagenet: A large-scale hierarchical image database. In *2009 IEEE Conference on Computer Vision and Pattern Recognition*, pages 248–255, 2009. doi: 10.1109/CVPR.2009.5206848.
- Prafulla Dhariwal and Alexander Nichol. Diffusion models beat gans on image synthesis. In M. Ranzato, A. Beygelzimer, Y. Dauphin, P.S. Liang, and J. Wortman Vaughan, editors, *Advances in Neural Information Processing Systems*, volume 34, pages 8780–8794. Curran Associates, Inc., 2021. URL <https://proceedings.neurips.cc/paper/2021/file/49ad23d1ec9fa4bd8d77d02681df5cfa-Paper.pdf>.
- Conor Durkan, Artur Bekasov, Iain Murray, and George Papamakarios. Neural spline flows. In H. Wallach, H. Larochelle, A. Beygelzimer, F. d'Alché-Buc, E. Fox, and R. Garnett, editors, *Advances in Neural Information Processing Systems*, volume 32. Curran Associates, Inc., 2019. URL <https://proceedings.neurips.cc/paper/2019/file/7ac71d433f282034e088473244df8c02-Paper.pdf>.
- Sergio Garrido, Stanislav Borysov, Jeppe Rich, and Francisco Pereira. Estimating causal effects with the neural autoregressive density estimator. *Journal of Causal Inference*, 9(1):211–218, 2021.
- Arthur Gretton, Kenji Fukumizu, Choon Teo, Le Song, Bernhard Schölkopf, and Alex Smola. A kernel statistical test of independence. In J. Platt, D. Koller, Y. Singer, and S. Roweis, editors, *Advances in Neural Information Processing Systems*, volume 20. Curran Associates, Inc., 2007. URL <https://proceedings.neurips.cc/paper/2007/file/d5cfead94f5350c12c322b5b664544c1-Paper.pdf>.
- Arthur Gretton, Karsten M. Borgwardt, Malte J. Rasch, Bernhard Schölkopf, and Alexander Smola. A kernel two-sample test. *Journal of Machine Learning Research*, 13(25):723–773, 2012. URL <http://jmlr.org/papers/v13/gretton12a.html>.
- Jonathan Ho and Tim Salimans. Classifier-free diffusion guidance. In *NeurIPS 2021 Workshop on Deep Generative Models and Downstream Applications*, 2021. URL <https://openreview.net/forum?id=qw8AKxfYbI>.
- Jonathan Ho, Ajay Jain, and Pieter Abbeel. Denoising diffusion probabilistic models. In H. Larochelle, M. Ranzato, R. Hadsell, M.F. Balcan, and H. Lin, editors, *Advances in Neural Information Processing Systems*, volume 33, pages 6840–6851. Curran Associates, Inc., 2020. URL <https://proceedings.neurips.cc/paper/2020/file/4c5bcfec8584af0d967f1ab10179ca4b-Paper.pdf>.

- Patrik Hoyer, Dominik Janzing, Joris M Mooij, Jonas Peters, and Bernhard Schölkopf. Nonlinear causal discovery with additive noise models. In D. Koller, D. Schuurmans, Y. Bengio, and L. Bottou, editors, *Advances in Neural Information Processing Systems*, volume 21. Curran Associates, Inc., 2008. URL <https://proceedings.neurips.cc/paper/2008/file/f7664060cc52bc6f3d620bcedc94a4b6-Paper.pdf>.
- Amir-Hossein Karimi, Julius Von Kügelgen, Bernhard Schölkopf, and Isabel Valera. Algorithmic recourse under imperfect causal knowledge: a probabilistic approach. *Advances in neural information processing systems*, 33: 265–277, 2020.
- Ilyes Khemakhem, Ricardo Monti, Robert Leech, and Aapo Hyvarinen. Causal autoregressive flows. In Arindam Banerjee and Kenji Fukumizu, editors, *Proceedings of The 24th International Conference on Artificial Intelligence and Statistics*, volume 130 of *Proceedings of Machine Learning Research*, pages 3520–3528. PMLR, 13–15 Apr 2021. URL <https://proceedings.mlr.press/v130/khemakhem21a.html>.
- Murat Kocaoglu, Christopher Snyder, Alexandros G Dimakis, and Sriram Vishwanath. Causalgan: Learning causal implicit generative models with adversarial training. In *International Conference on Learning Representations*, 2018.
- Zhifeng Kong, Wei Ping, Jiaji Huang, Kexin Zhao, and Bryan Catanzaro. Diffwave: A versatile diffusion model for audio synthesis. In *International Conference on Learning Representations*, 2021. URL <https://openreview.net/forum?id=a-xFK8Ymz5J>.
- Joris Mooij, Dominik Janzing, Jonas Peters, and Bernhard Schölkopf. Regression by dependence minimization and its application to causal inference in additive noise models. In *Proceedings of the 26th Annual International Conference on Machine Learning, ICML '09*, page 745–752, New York, NY, USA, 2009. Association for Computing Machinery. ISBN 9781605585161. doi: 10.1145/1553374.1553470. URL <https://doi.org/10.1145/1553374.1553470>.
- Raha Moraffah, Bahman Moraffah, Mansooreh Karami, Adrienne Raglin, and Huan Liu. Can: A causal adversarial network for learning observational and interventional distributions. *arXiv preprint arXiv:2008.11376*, 2020.
- Krikamol Muandet, Motonobu Kanagawa, Sorawit Saengkyongam, and Sanparith Marukatat. Counterfactual mean embeddings. *J. Mach. Learn. Res.*, 22:162–1, 2021.
- Alexander Quinn Nichol and Prafulla Dhariwal. Improved denoising diffusion probabilistic models. In Marina Meila and Tong Zhang, editors, *Proceedings of the 38th International Conference on Machine Learning*, volume 139 of *Proceedings of Machine Learning Research*, pages 8162–8171. PMLR, 18–24 Jul 2021. URL <https://proceedings.mlr.press/v139/nichol21a.html>.
- Álvaro Parafita and Jordi Vitrià. Causal inference with deep causal graphs. *arXiv preprint arXiv:2006.08380*, 2020.
- Nick Pawlowski, Daniel Coelho de Castro, and Ben Glocker. Deep structural causal models for tractable counterfactual inference. *Advances in Neural Information Processing Systems*, 33:857–869, 2020.
- J. Pearl, M. Glymour, and N.P. Jewell. *Causal Inference in Statistics: A Primer*. Wiley, 2016. ISBN 9781119186847. URL <https://books.google.com/books?id=L3G-CgAAQBAJ>.
- Judea Pearl. Causal inference in statistics: An overview. *Statistics Surveys*, 3(none):96 – 146, 2009. doi: 10.1214/09-SS057. URL <https://doi.org/10.1214/09-SS057>.
- Jonas Peters, Dominik Janzing, and Bernhard Schölkopf. *Elements of causal inference: foundations and learning algorithms*. The MIT Press, 2017.
- Aditya Ramesh, Prafulla Dhariwal, Alex Nichol, Casey Chu, and Mark Chen. Hierarchical text-conditional image generation with clip latents. 2022. URL <https://arxiv.org/abs/2204.06125>.
- Saptarshi Saha and Utpal Garain. On noise abduction for answering counterfactual queries: A practical outlook. *Transactions on Machine Learning Research*.

- Chitwan Saharia, William Chan, Saurabh Saxena, Lala Li, Jay Whang, Emily Denton, Seyed Kamyar Seyed Ghasemipour, Burcu Karagol Ayan, S. Sara Mahdavi, Rapha Gontijo Lopes, Tim Salimans, Jonathan Ho, David J Fleet, and Mohammad Norouzi. Photorealistic text-to-image diffusion models with deep language understanding. 2022. URL <https://arxiv.org/abs/2205.11487>.
- Pedro Sanchez and Sotirios A. Tsafaris. Diffusion causal models for counterfactual estimation. In *CLear*, 2022.
- Pablo Sánchez-Martín, Miriam Rateike, and Isabel Valera. Vaca: Design of variational graph autoencoders for interventional and counterfactual queries. *ArXiv*, abs/2110.14690, 2021.
- Uri Shalit, Fredrik D Johansson, and David Sontag. Estimating individual treatment effect: generalization bounds and algorithms. In *International Conference on Machine Learning*, pages 3076–3085. PMLR, 2017.
- Amit Sharma, Emre Kiciman, et al. DoWhy: A Python package for causal inference. <https://github.com/microsoft/dowhy>, 2019.
- Jascha Sohl-Dickstein, Eric Weiss, Niru Maheswaranathan, and Surya Ganguli. Deep unsupervised learning using nonequilibrium thermodynamics. In Francis Bach and David Blei, editors, *Proceedings of the 32nd International Conference on Machine Learning*, volume 37 of *Proceedings of Machine Learning Research*, pages 2256–2265, Lille, France, 07–09 Jul 2015. PMLR. URL <https://proceedings.mlr.press/v37/sohl-dickstein15.html>.
- Jiaming Song, Chenlin Meng, and Stefano Ermon. Denoising diffusion implicit models. In *International Conference on Learning Representations*, 2021. URL <https://openreview.net/forum?id=StlgIarCHLP>.
- Peter Spirtes, Clark N Glymour, Richard Scheines, and David Heckerman. *Causation, prediction, and search*. MIT press, 2000.
- W. H. Thompson, R. Nair, H. Oya, O. Esteban, J. M. Shine, C. I. Petkov, R. A. Poldrack, M. Howard, and R. Adolphs. A data resource from concurrent intracranial stimulation and functional MRI of the human brain. *Scientific Data*, 7(1):258, August 2020. ISSN 2052-4463. doi: 10.1038/s41597-020-00595-y. URL <https://doi.org/10.1038/s41597-020-00595-y>.
- Matej Zečević, Devendra Dhama, Athresh Karanam, Sriraam Natarajan, and Kristian Kersting. Interventional sum-product networks: Causal inference with tractable probabilistic models. *Advances in Neural Information Processing Systems*, 34:15019–15031, 2021.
- Kun Zhang and Aapo Hyvarinen. On the identifiability of the post-nonlinear causal model. *arXiv preprint arXiv:1205.2599*, 2012.

Appendix

A Encoding and Decoding

Algorithm 4 $\text{Enc}_i(X_i, X_{\text{pa}_i})$

Input: X_i, X_{pa_i}

- 1: $Z_i^0 \leftarrow X_i$
 - 2: **for** $t = 0, \dots, T - 1$ **do**
 - 3: $Z_i^{t+1} \leftarrow \sqrt{\frac{\alpha_{t+1}}{\alpha_t}} Z_i^t + \varepsilon_\theta^i(Z_i^t, X_{\text{pa}_i}, t) \left(\sqrt{1 - \alpha_{t+1}} - \sqrt{\frac{\alpha_{t+1}(1 - \alpha_t)}{\alpha_t}} \right)$
 - 4: **end for**
 - 5: **Return** Z_i^T
-

Algorithm 5 $\text{Dec}_i(Z_i, X_{\text{pa}_i})$

Input: Z_i, X_{pa_i}

- 1: $\hat{X}_i^T \leftarrow Z_i$
 - 2: **for** $t = T, \dots, 1$ **do**
 - 3: $\hat{X}_i^{t-1} \leftarrow \sqrt{\frac{\alpha_{t-1}}{\alpha_t}} \hat{X}_i^t - \varepsilon_\theta^i(\hat{X}_i^t, X_{\text{pa}_i}, t) \left(\sqrt{\frac{\alpha_{t-1}(1 - \alpha_t)}{\alpha_t}} - \sqrt{1 - \alpha_{t-1}} \right)$
 - 4: **end for**
 - 5: **Return** \hat{X}_i^0
-

B Missing Details from Section 4

Notation. For two sets \mathcal{X}, \mathcal{Y} a map $f : \mathcal{X} \mapsto \mathcal{Y}$, and a set $S \subset \mathcal{X}$, we define $f(S) = \{f(x) : x \in S\}$. For $x \in \mathcal{X}$, we define $x + S = \{x + x' : x' \in S\}$. For a random variable X , define $p_X(x)$ as the probability density function (pdf) at x . We use p.d. to denote positive definite matrices and $Jf|_x$ to denote the Jacobian of f evaluated at x . For a function with two inputs $f(\cdot, \cdot)$, we define $f_x(Y) = f(x, Y)$ and $f_y(X) = f(X, y)$.

Lemma 2. For $\mathcal{U}, \mathcal{Z} \subset \mathbb{R}$, consider a family of invertible functions $q_{x_{\text{pa}}} : \mathcal{U} \rightarrow \mathcal{Z}$ for $x_{\text{pa}} \in \mathcal{X}_{\text{pa}} \subset \mathbb{R}^d$, then $\frac{dq_{x_{\text{pa}}}}{du}(q_{x_{\text{pa}}}^{-1}(z)) = c(z)$ for all $x_{\text{pa}} \in \mathcal{X}_{\text{pa}}$ if and only if $q_{x_{\text{pa}}}$ can be expressed as

$$q_{x_{\text{pa}}}(u) = q(u + r(x_{\text{pa}}))$$

for some function r and invertible q .

Proof. First for the reverse direction, we may assume $q_{x_{\text{pa}}}(u) = q(u + r(x_{\text{pa}}))$. Then

$$\frac{dq_{x_{\text{pa}}}}{du}(u) = \frac{dq}{du}(u + r(x_{\text{pa}})).$$

Now plugging in $u = q_{x_{\text{pa}}}^{-1}(z) = q^{-1}(z) - r(x_{\text{pa}})$,

$$\frac{dq_{x_{\text{pa}}}}{du}(q_{x_{\text{pa}}}^{-1}(z)) = \frac{dq}{du}(q^{-1}(z) - r(x_{\text{pa}}) + r(x_{\text{pa}})) = \frac{dq}{du}(q^{-1}(z)) = c(z).$$

Therefore $\frac{dq_{x_{\text{pa}}}}{du}(q_{x_{\text{pa}}}^{-1}(z))$ is a function of z .

For the forward direction, assume $\frac{dq_{x_{\text{pa}}}}{du}(q_{x_{\text{pa}}}^{-1}(z)) = c(z)$. Define $s_{x_{\text{pa}}} : \mathcal{Z} \rightarrow \mathcal{U}$ to be the inverse of $q_{x_{\text{pa}}}$. By the inverse function theorem and by assumption.

$$\frac{ds_{x_{\text{pa}}}}{dz}(z) = \frac{dq_{x_{\text{pa}}}^{-1}}{dz}(z) = \frac{1}{\frac{dq_{x_{\text{pa}}}}{du}(q_{x_{\text{pa}}}^{-1}(z))} = \frac{1}{c(z)}$$

for all x_{pa} . Since the derivatives of $s_{x_{\text{pa}}}$ are equal for all x_{pa} , by the mean value theorem, all $s_{x_{\text{pa}}}$ are additive shifts of each other. Without loss of generality, we may consider an arbitrary fixed $x_{\text{pa}_0} \in \mathcal{X}_{\text{pa}}$ and reparametrize $s_{x_{\text{pa}}}$ as

$$s_{x_{\text{pa}}}(z) = s_{x_{\text{pa}_0}}(z) - r(x_{\text{pa}}).$$

Let $u = s_{x_{\text{pa}_0}}(z)$. Then we have

$$\begin{aligned} s_{x_{\text{pa}_0}}(z) &= u + r(x_{\text{pa}_0}) \\ q_{x_{\text{pa}}}(u) &= z = q_{x_{\text{pa}_0}}(u + r(x_{\text{pa}})), \end{aligned}$$

and we have the desired representation by choosing $q = q_{x_{\text{pa}_0}}$. \square

Theorem 1. Assume for $X \in \mathcal{X} \subset \mathbb{R}$ and exogenous noise $U \sim \text{Unif}[0, 1]$, X satisfies the structural equation: $X = f(X_{\text{pa}}, U)$, where $X_{\text{pa}} \in \mathcal{X}_{\text{pa}} \subset \mathbb{R}^d$ are the parents of node X and $U \perp\!\!\!\perp X_{\text{pa}}$.

Consider an encoder-decoder model with encoding function $g : \mathcal{X} \times \mathcal{X}_{\text{pa}} \rightarrow \mathcal{Z}$ and decoding function $h : \mathcal{Z} \times \mathcal{X}_{\text{pa}} \rightarrow \mathcal{X}$,

$$Z = g(X, X_{\text{pa}}), \quad \hat{X} = h(Z, X_{\text{pa}}).$$

Assume the following conditions are met:

1. The encoding is independent from the parent values, $g(X, X_{\text{pa}}) \perp\!\!\!\perp X_{\text{pa}}$.
2. Under some metric d e.g., $\|\cdot\|_2$, the model has reconstruction error less than τ ,

$$d(h(g(X, X_{\text{pa}}), X_{\text{pa}}), X) \leq \tau. \quad (4)$$

3. The structural equation f is invertible, differentiable, and increasing with respect to U .
4. The encoding g is invertible and differentiable with respect to X .

Then for a sample (x_{pa}, x, u) and intervention $\text{do}(X_{\text{pa}} := \gamma)$, the counterfactual estimate from the model of the true counterfactual $x^{\text{CF}} = f(\gamma, u)$ has estimation error at most τ : $d(h(g(x, x_{\text{pa}}), \gamma), x^{\text{CF}}) \leq \tau$.

Proof. We show that $g(X, X_{\text{pa}}) = g(f(X_{\text{pa}}, U), X_{\text{pa}})$ is solely a function of U .

Since continuity and invertibility imply monotonicity, without loss of generality, assume g is an increasing function (if not, we may replace g with $-g$ and use $h(-Z, X_{\text{pa}})$). By properties of the composition of functions, $q_{x_{\text{pa}}}(U) := g(f(x_{\text{pa}}, U), x_{\text{pa}})$ is also invertible, differentiable, and increasing with respect to U .

By the assumption that the encoding Z is independent of X_{pa} ,

$$Z = q_{x_{\text{pa}}}(U) \perp\!\!\!\perp X_{\text{pa}}. \quad (5)$$

Therefore the conditional distribution of Z does not depend on X_{pa} . Using the assumption that $U \perp\!\!\!\perp X_{\text{pa}}$, for all $x_{\text{pa}} \in \mathcal{X}_{\text{pa}}$ and z in the support of Z , by the change of density formula,

$$p_Z(z) = \frac{p_U(q_{x_{\text{pa}}}^{-1}(z))}{\left| \frac{dq_{x_{\text{pa}}}}{du}(q_{x_{\text{pa}}}^{-1}(z)) \right|} = \frac{\mathbb{1}\{q_{x_{\text{pa}}}^{-1}(z) \in [0, 1]\}}{\frac{dq_{x_{\text{pa}}}}{du}(q_{x_{\text{pa}}}^{-1}(z))} = c_1(z). \quad (6)$$

The numerator follows from the fact that the noise is uniformly distributed. The term $\frac{dq_{x_{\text{pa}}}}{du}(q_{x_{\text{pa}}}^{-1}(z))$ is nonnegative since $q_{x_{\text{pa}}}$ is increasing. Furthermore, since $p_Z(z) > 0$, the numerator in Eq. (6) is always equal to 1 and the denominator must not depend on X_{pa} ,

$$\frac{dq_{x_{\text{pa}}}}{du}(q_{x_{\text{pa}}}^{-1}(z)) = c_2(z)$$

for some function c_2 . From Lemma 2 (by replacing a by x_{pa}), we may express

$$q_{x_{\text{pa}}}(u) = q(u + r(x_{\text{pa}})) \quad (7)$$

for an invertible function q .

Next, since $Z \perp\!\!\!\perp X_{\text{pa}}$, the support of Z does not depend on X_{pa} , equivalently the ranges of q_{x_1} and q_{x_2} are equal for all $x_1, x_2 \in \mathcal{X}_{\text{pa}}$,

$$q_{x_1}([0, 1]) = q_{x_2}([0, 1]). \quad (8)$$

Applying Eq. (7) and the invertibility of q ,

$$\begin{aligned} q([0, 1] + r(x_1)) &= q([0, 1] + r(x_2)) \\ [0, 1] + r(x_1) &= [0, 1] + r(x_2) \\ [r(x_1), r(x_1) + 1] &= [r(x_2), r(x_2) + 1] \end{aligned}$$

Since this holds for all $x_1, x_2 \in \mathcal{X}_{\text{pa}}$, we have $r(x_{\text{pa}})$ is a constant function, or $r(x_{\text{pa}}) \equiv r$. Thus let \tilde{q} be $\tilde{q}(u) = q(u + r) = q_{x_{\text{pa}}}(u)$, which is solely a function of U for all x_{pa} . For all x_{pa} ,

$$g(f(x_{\text{pa}}, U), x_{\text{pa}}) = q_{x_{\text{pa}}}(U) = \tilde{q}(U) \implies g(f(X_{\text{pa}}, U), X_{\text{pa}}) = \tilde{q}(U). \quad (9)$$

Lastly, for the intervention $\text{do}(X_{\text{pa}} := \gamma)$, the counterfactual sample is $(\gamma, x^{\text{CF}}, u)$ where $x^{\text{CF}} = f(\gamma, u)$. Since Eq. (9) holds true for all X_{pa} and U , it holds for the factual and counterfactual samples,

$$g(x, x_{\text{pa}}) = g(f(x_{\text{pa}}, u), x_{\text{pa}}) = \tilde{q}(u) = g(f(\gamma, u), \gamma) = g(x^{\text{CF}}, \gamma). \quad (10)$$

By applying equations Eqs. (4) and (10),

$$d(h(g(x^{\text{CF}}, \gamma), \gamma), x^{\text{CF}}) \leq \tau \quad (11)$$

$$d(h(g(x, x_{\text{pa}}), \gamma), x^{\text{CF}}) \leq \tau. \quad (12)$$

□

B.1 Multivariate Setting

Theorem 3. Assume for $X \in \mathcal{X} \subset \mathbb{R}^m$ and continuous exogenous noise $U \sim \text{Unif}[0, 1]^m$ for $m \geq 3$, and X satisfies the structural equation

$$X = f(X_{\text{pa}}, U) \quad (13)$$

where $X_{\text{pa}} \in \mathcal{X}_{\text{pa}} \subset \mathbb{R}^d$ are the parents of node X and $U \perp\!\!\!\perp X_{\text{pa}}$. Consider an encoder-decoder model with encoding function $g : \mathcal{X} \times \mathcal{X}_{\text{pa}} \rightarrow \mathcal{Z}$ and decoding function $h : \mathcal{Z} \times \mathcal{X}_{\text{pa}} \rightarrow \mathcal{X}$,

$$Z = g(X, X_{\text{pa}}), \quad \hat{X} = h(Z, X_{\text{pa}}). \quad (14)$$

Assume the following conditions are met:

1. The encoding is independent from the parent values, $g(X, X_{\text{pa}}) \perp\!\!\!\perp X_{\text{pa}}$.
2. Under metric d e.g. $\|\cdot\|_2$, the model has reconstruction error less than τ ,

$$d(h(g(X, X_{\text{pa}}), X_{\text{pa}}), X) \leq \tau. \quad (15)$$

3. The structural equation f is invertible and differentiable with respect to U , and $Jf_{x_{\text{pa}}}$ is p.d. for all $x_{\text{pa}} \in \mathcal{X}_{\text{pa}}$.
4. The encoding g is invertible and differentiable with respect to X , and $Jg_{x_{\text{pa}}}$ is p.d. for all $x_{\text{pa}} \in \mathcal{X}_{\text{pa}}$.
5. The encoding $q_{x_{\text{pa}}}(U) := g(f(x_{\text{pa}}, U), x_{\text{pa}})$ satisfies $Jq_{x_{\text{pa}}} |_{q_{x_{\text{pa}}}^{-1}(z)} = c(x_{\text{pa}})A$ for all $z \in \mathcal{Z}$ and $x_{\text{pa}} \in \mathcal{X}_{\text{pa}}$, where c is a scalar function and A is an orthogonal matrix.

Then for a sample (x_{pa}, x, u) and intervention $\text{do}(X_{\text{pa}} = \gamma)$, the counterfactual estimate from the model of the true counterfactual $x^{\text{CF}} = f(\gamma, u)$ has estimation error at most τ ,

$$d(h(g(x, x_{\text{pa}}), \gamma), x^{\text{CF}}) \leq \tau. \quad (16)$$

Proof. We may show that $g(X, X_{\text{pa}}) = g(f(X_{\text{pa}}, U), X_{\text{pa}})$ is solely a function of U .

By properties of composition of functions, $q_{x_{\text{pa}}}(U) := g(f(x_{\text{pa}}, U), x_{\text{pa}})$ is also invertible, differentiable. Since $Jf_{x_{\text{pa}}}$ and $Jg_{x_{\text{pa}}}$ are p.d. and $Jq_{x_{\text{pa}}} = Jf_{x_{\text{pa}}}Jg_{x_{\text{pa}}}$, then $Jq_{x_{\text{pa}}}$ is p.d. for all $x_{\text{pa}} \in \mathcal{X}_{\text{pa}}$ as well.

By the assumption that the encoding Z is independent of X_{pa} ,

$$Z = q_{X_{\text{pa}}}(U) \perp\!\!\!\perp X_{\text{pa}}. \quad (17)$$

Therefore the conditional distribution of Z does not depend on X_{pa} . Using the assumption that $U \perp\!\!\!\perp X_{\text{pa}}$, for all $x_{\text{pa}} \in \mathcal{X}_{\text{pa}}$ and z in the support of Z , by the change of density formula,

$$p_Z(z) = \frac{p_U(q_{x_{\text{pa}}}^{-1}(z))}{\left| \det Jq_{x_{\text{pa}}} |_{q_{x_{\text{pa}}}^{-1}(z)} \right|} = \frac{2^{-m} \mathbb{1}\{q_{x_{\text{pa}}}^{-1}(z) \in [0, 1]^m\}}{\det Jq_{x_{\text{pa}}} |_{q_{x_{\text{pa}}}^{-1}(z)}} = c_1(z). \quad (18)$$

The numerator follows from the fact that the noise is uniformly distributed. The determinant of the Jacobian term $Jq_{x_{\text{pa}}}(q_{x_{\text{pa}}}^{-1}(z))$ is nonnegative since $Jq_{x_{\text{pa}}}$ is p.d. Furthermore, since $p_Z(z) > 0$, the numerator in Eq. (18) is always equal to 2^{-m} and the denominator must not depend on X_{pa} ,

$$\det Jq_{x_{\text{pa}}} |_{q_{x_{\text{pa}}}^{-1}(z)} = c_2(z) \quad (19)$$

for some function c_2 . From our assumption, $Jq_{x_{\text{pa}}} |_{q_{x_{\text{pa}}}^{-1}(z)} = c(x_{\text{pa}})A$ for an orthogonal matrix A for all z . Applying this to Eq. (19),

$$\det Jq_{x_{\text{pa}}} |_{q_{x_{\text{pa}}}^{-1}(z)} = \det c(x_{\text{pa}})A = c(x_{\text{pa}}) = c_2(z),$$

which implies $c(x_{\text{pa}}) \equiv c$ is a constant function, or $Jq_{x_{\text{pa}}} |_{q_{x_{\text{pa}}}^{-1}(z)} = cA$. By Lemma 4, we may express $q_{x_{\text{pa}}}(u)$ as

$$q_{x_{\text{pa}}}(u) = q(u + r(x_{\text{pa}})) \quad (20)$$

for an invertible function q .

Next, since $Z \perp\!\!\!\perp X_{\text{pa}}$, the support of Z does not depend on X_{pa} , equivalently the ranges of $q_{x_{\text{pa}_1}}$ and $q_{x_{\text{pa}_2}}$ are equal for all $x_1, x_2 \in \mathcal{X}_{\text{pa}}$,

$$q_{x_1}([0, 1]^m) = q_{x_2}([0, 1]^m). \quad (21)$$

Applying Eq. (20) and the invertibility of q ,

$$\begin{aligned} q([0, 1]^m + r(x_1)) &= q([0, 1]^m + r(x_2)) \\ [0, 1]^m + r(x_1) &= [0, 1]^m + r(x_2) \\ [r(x_1), r(x_1) + 1]^m &= [r(x_2), r(x_2) + 1]^m. \end{aligned}$$

Since this holds for all $x_1, x_2 \in \mathcal{X}_{\text{pa}}$, we have $r(x)$ is a constant, or $r(x) \equiv r$. Thus let \tilde{q} be $\tilde{q}(u) = q(u + r) = q_{x_{\text{pa}}}(u)$, which is solely a function of U for all x_{pa} . For all x_{pa} ,

$$g(f(x_{\text{pa}}, U), x_{\text{pa}}) = q_{x_{\text{pa}}}(U) = \tilde{q}(U) \implies g(f(X_{\text{pa}}, U), X_{\text{pa}}) = \tilde{q}(U). \quad (22)$$

Lastly, for the intervention $\text{do}(X_{\text{pa}} = \gamma)$, the counterfactual sample is $(\gamma, x^{\text{CF}}, u)$ where $x^{\text{CF}} = f(\gamma, u)$. Since Eq. (22) holds true for all X_{pa} and U , it holds for the factual and counterfactual samples,

$$g(x, x_{\text{pa}}) = g(f(x_{\text{pa}}, u), x_{\text{pa}}) = \tilde{q}(u) = g(f(\gamma, u), \gamma) = g(x^{\text{CF}}, \gamma). \quad (23)$$

By applying Eqs. (15) and (23),

$$\begin{aligned} d(h(g(x^{\text{CF}}, \gamma), \gamma), x^{\text{CF}}) &\leq \tau \\ d(h(g(x, x_{\text{pa}}), \gamma), x^{\text{CF}}) &\leq \tau. \end{aligned}$$

□

Lemma 4. For $\mathcal{U}, \mathcal{Z} \subset \mathbb{R}^m$, consider a family of invertible functions $q_{x_{\text{pa}}} : \mathcal{U} \rightarrow \mathcal{Z}$ for $x_{\text{pa}} \in \mathcal{X}_{\text{pa}} \subset \mathbb{R}^d$, if $Jq_{x_{\text{pa}}}(q_{x_{\text{pa}}}^{-1}(z)) = cA$ for all $x_{\text{pa}} \in \mathcal{X}_{\text{pa}}$ then $q_{x_{\text{pa}}}$ can be expressed as

$$q_{x_{\text{pa}}}(u) = q(u + r(x_{\text{pa}}))$$

for some function r and invertible q .

Proof. Assume $Jq_{x_{\text{pa}}}(q_{x_{\text{pa}}}^{-1}(z)) = cA$. By the inverse function theorem,

$$Jq_{x_{\text{pa}}}^{-1}|_z = \left(Jq_{x_{\text{pa}}}|_{q_{x_{\text{pa}}}^{-1}(z)} \right)^{-1}. \quad (24)$$

Define $s_{x_{\text{pa}}} : \mathcal{Z} \rightarrow \mathcal{U}$ to be the inverse of $q_{x_{\text{pa}}}$. By assumption

$$\det Jq_{x_{\text{pa}}}|_{q_{x_{\text{pa}}}^{-1}(z)} = \det Jq_{x_{\text{pa}}}^{-1}|_z = \det Js_{x_{\text{pa}}}|_z = cA$$

for all x_{pa} and a constant c and orthogonal matrix A . Since the Jacobian of $s_{x_{\text{pa}}}$ is a scaled orthogonal matrix, $s_{x_{\text{pa}}}$ is a conformal function. Therefore by Liouville's theorem, $s_{x_{\text{pa}}}$ is a Möbius function [Blair, 2000], which implies that

$$s_{x_{\text{pa}}}(z) = b_{x_{\text{pa}}} + \alpha_{x_{\text{pa}}} A_{x_{\text{pa}}}(z - a_{x_{\text{pa}}}) / \|z - a_{x_{\text{pa}}}\|^\varepsilon, \quad (25)$$

where $A_{x_{\text{pa}}}$ is an orthogonal matrix, $\varepsilon \in \{0, 2\}$, $a_{x_{\text{pa}}} \in \mathbb{R}^m$, and $\alpha_{x_{\text{pa}}} \in \mathbb{R}$. The Jacobian of $s_{x_{\text{pa}}}$ is equal to cA by assumption

$$Js_{x_{\text{pa}}}|_z = \frac{\alpha_{x_{\text{pa}}} A_{x_{\text{pa}}}}{\|z - a_{x_{\text{pa}}}\|^\varepsilon} \left(I - \varepsilon \frac{(z - a_{x_{\text{pa}}})(z - a_{x_{\text{pa}}})^T}{\|z - a_{x_{\text{pa}}}\|^2} \right) = cA.$$

This imposes constraints on variables α , a , and ε . Choose z such that $z - a_{x_{\text{pa}}} = kv$ for a unit vector v and multiply by $A_{x_{\text{pa}}}^{-1}$,

$$\begin{aligned} cAA_{x_{\text{pa}}}^{-1} &= \frac{\alpha_{x_{\text{pa}}}}{\|kv\|^\varepsilon} \left(I - \varepsilon \frac{k^2 vv^T}{k^2 \|v\|^2} \right) \\ I &= \varepsilon vv^T + \left(\frac{ck^\varepsilon}{\alpha_{x_{\text{pa}}}} \right) AA_{x_{\text{pa}}}^{-1}. \end{aligned}$$

If $\varepsilon = 2$, choosing different values of k , implying different values of z , results in varying values of on the right hand side, which should be the constant identity matrix. Therefore we must have $\varepsilon = 0$. This also implies that $\alpha_{x_{\text{pa}}} = c$ and $A = A_{x_{\text{pa}}}$. This gives the further parametrization

$$s_{x_{\text{pa}}}(z) = b_{x_{\text{pa}}} - cA(z - a_{x_{\text{pa}}}) = b'(x_{\text{pa}}) + cAz$$

where $b'(x_{\text{pa}}) = b_{x_{\text{pa}}} - cAa_{x_{\text{pa}}}$.

Without loss of generality, we may consider an arbitrary fixed $x_{\text{pa}_0} \in \mathcal{X}_{\text{pa}}$,

$$s_{x_{\text{pa}_0}}(z) - s_{x_{\text{pa}}}(z) = r(x_{\text{pa}}) := b'(x_{\text{pa}_0}) - b'(x_{\text{pa}}).$$

Let $u = s_{x_{\text{pa}}}(z)$. Then we have

$$\begin{aligned} s_{x_{\text{pa}_0}}(z) &= u + r(x_{\text{pa}}) \\ q_{x_{\text{pa}}}(u) &= z = q_{x_{\text{pa}_0}}(u + r(x_{\text{pa}})), \end{aligned}$$

and we have the desired representation by choosing $q = q_{x_{\text{pa}_0}}$. □

C Additional Experimental Details

C.1 Details about the Additive Noise Model (ANM)

For a given node X with parents X_{pa} , consider fitting a regression model \hat{f} where $\hat{f}(X_{\text{pa}}) \approx X$. Using this regression model and the training dataset is sufficient for generating samples from the observational and interventional distribution as well as computing counterfactuals.

Observational/Interventional Samples. Samples are constructed in topological order. For intervened nodes, the sampled value is always the intervened value. Non-intervened root nodes in the SCM are sampled from the empirical distribution of the training set. For a non-intervened non-root node i with parents pa_i with regression model \hat{f}_i , let $(X_{i,1}, \dots, X_{i,n})$ and $(X_{\text{pa}_{i,1}}, \dots, X_{\text{pa}_{i,n}})$ be the training set. Let $\hat{U}_j = X_{i,j} - \hat{f}_i(X_{\text{pa}_{i,j}})$ be the residual for the j th sample in the training set. A new sample for X_i is generated by sampling the parent value X_{pa_i} inductively and sampling \hat{U} from the empirical residual distribution $(\hat{U}_1, \dots, \hat{U}_n)$, and outputting $\hat{f}(X_{\text{pa}_i}) + \hat{U}$.

Counterfactual Estimation. For a factual observation X^F and interventions on nodes \mathcal{I} with values γ , the counterfactual estimate only differs from the factual estimate for all nodes that are intervened or downstream from an intervened node. Similarly for observation and interventional samples, we proceed in topological order. For each intervened node i , $X_i^{\text{CF}} = \gamma_i$. For each non-intervened node i downstream from an intervened node, define $\hat{U}_i^F = X_i^F - \hat{f}_i(X_{\text{pa}_i}^F)$, the residual and estimated noise for the factual sample. Let $X_{\text{pa}_i}^{\text{CF}}$ be counterfactual estimates of the parents of X_i . Then $X_i^{\text{CF}} = \hat{f}_i(X_{\text{pa}_i}^{\text{CF}}) + \hat{U}_i^F$.

Therefore for counterfactual queries, if the true functional equation f_i is an additive noise model, then if $\hat{f}_i \approx f_i$, the regression model will have low counterfactual error. In fact, if $\hat{f}_i \equiv f_i$, then the regression model will have perfect counterfactual performance.

C.2 Structural Equations

To select structural equations for our synthetic datasets, we decided to balance the effect of the unobserved exogenous noise. Consider a node with value X with parent values $\text{pa}(X)$ and exogenous noise U where $\text{pa}(X) \perp\!\!\!\perp U$, and corresponding functional equation f such that

$$X = f(\text{pa}(X), U).$$

Further assuming the additive noise model, $X = f_1(\text{pa}(X)) + f_2(U)$. In this additive setting, since $\text{pa}(X) \perp\!\!\!\perp U$, we have

$$\text{Var}[X] = \text{Var}[f_1(\text{pa}(X))] + \text{Var}[f_2(U)].$$

We choose f_1 and f_2 such that

$$0.05 \leq \frac{\text{Var}[f_2(U)]}{\text{Var}[f_1(\text{pa}(X))]} \leq 0.5,$$

representing the fact that the ratio of the effect of the noise to the parents is roughly approximate or smaller by an order of magnitude.

For the nonadditive case, we decompose the variance using the law of total variance,

$$\text{Var}[X] = \mathbb{E} \text{Var}[f(\text{pa}(X), U) | U] + \text{Var} \mathbb{E}[f(\text{pa}(X), U) | U].$$

Similarly, we choose the functional equation f such that f satisfies

$$0.05 \leq \frac{\text{Var} \mathbb{E}[f(\text{pa}(X), U) | U]}{\mathbb{E} \text{Var}[f(\text{pa}(X), U) | U]} \leq 0.5$$

For all graphs, $U_i \stackrel{\text{iid}}{\sim} \mathcal{N}(0, 1)$, and we choose f such that $X_i = U_i$ if X_i is a root node, i.e. f is the identity function. Lastly, we normalize every node X_i such that $\text{Var}(X_i) \approx 1$. For the sake of clarity, we omit all normalizing terms in the formulas and omit functional equations for root nodes below.

SCM		Nonlinear Case	Nonadditive Case
<i>Chain</i>	$f_2(U_2, X_1)$	$\exp(X_1/2) + U_2/4$	$1/((U_2 + X_1)^2 + 0.5)$
	$f_3(U_3, X_2)$	$(X_2 - 5)^3/15 + U_3$	$\sqrt{X_2 + U_3 }/(0.1 + X_2)$
<i>Triangle</i>	$f_2(U_2, X_1)$	$2X_1^2 + U_2$	$X_1/((U_2 + X_1)^2 + 1) + U_2/4$
	$f_3(U_3, X_1, X_2)$	$20/(1 + \exp(-X_2^2 + X_1)) + U_3$	$(U_3 + 0.3)(-X_1 + X_2/2 + U_3 /5)^2$
<i>Diamond</i>	$f_2(U_2, X_1)$	$X_1^2 + U_2/2$	$\sqrt{ X_1 }(U_2 + 0.1)/2 + X_1 + U_2/5$
	$f_3(U_3, X_1, X_2)$	$X_2^2 - 2/(1 + \exp(-X_1)) + U_3/2$	$1/(1 + (U_3 + 0.5) \exp(-X_2 + X_1))$
	$f_4(U_4, X_2, X_3)$	$X_3/(X_2 + 2 + X_3 + 0.5) + U_4/10$	$(X_3 + X_2 + U_4/4 - 7)^2 - 20$
<i>Y</i>	$f_3(U_3, X_1, X_2)$	$4/(1 + \exp(-X_1 - X_2)) - X_2^2 + U_3/2$	$(X_1 - 2X_2 - 2)(U_3 + 0.2)$
	$f_4(U_4, X_3)$	$20/(1 + \exp(X_3^2/2 - X_3)) + U_4$	$(\cos(X_3) + U_4/2)^2$

Table 3: The equations defining the data generating process in the nonlinear and the nonadditive cases.

C.3 Model Hyperparameters

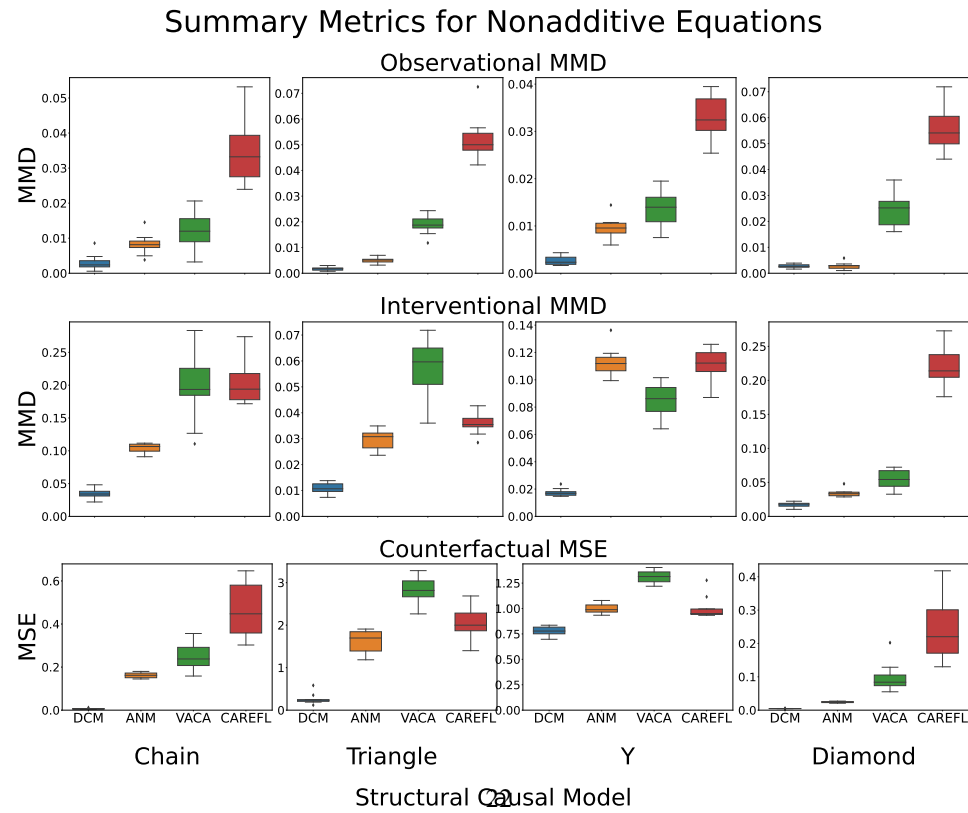
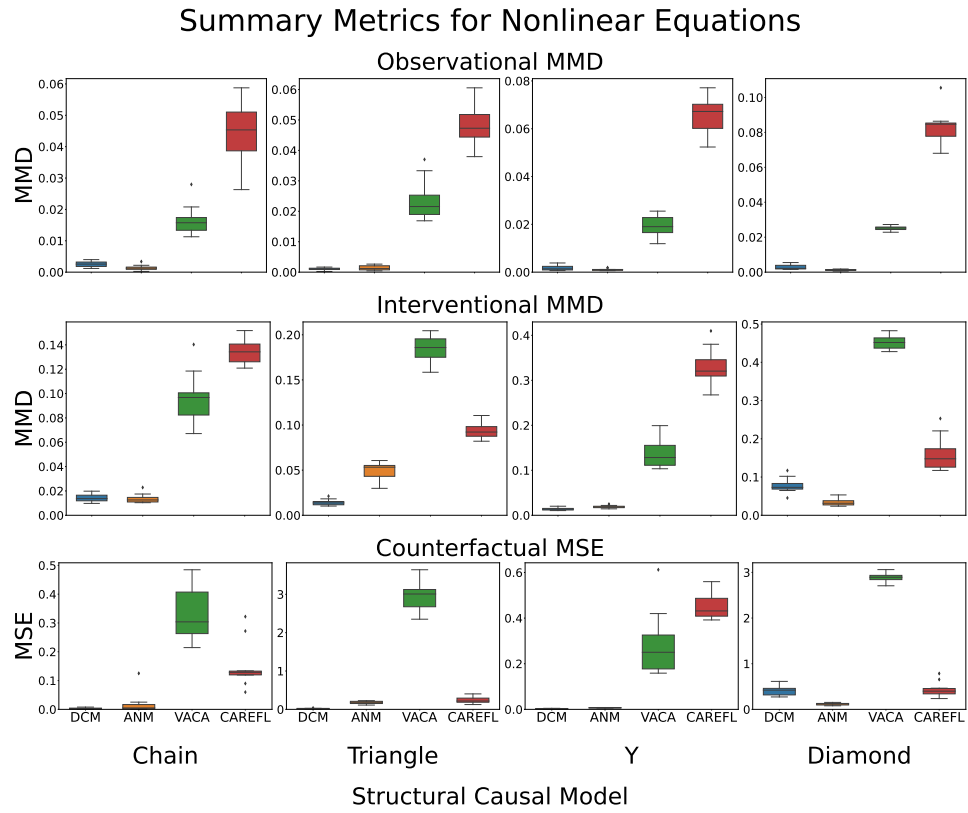
For all experiments in our evaluation, we hold the model hyperparameters constant. For DCM, we use the default hyperparameters and implementation from Section 5.

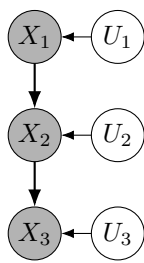
For VACA, we use the default implementation, training for 500 epochs, with a learning rate of 0.005, and the encoder and decoder have hidden dimensions of size [8, 8] and [16] respectively, a latent vector dimension of 4, and a parent dropout rate of 0.2.

For CAREFL, we also use the default implementation with the neural spline autoregressive flows [Durkan et al., 2019], training for 500 epochs with a learning rate of 0.005, four flows, and ten hidden units.

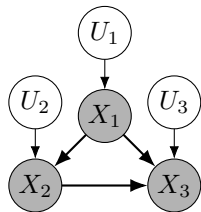
For ANM, we also use the default implementation to select a regression model. Given a set of fitted regression models, the ANM chooses the model with the lowest root mean squared error averaged over splits of the data. The ANM considers the following regressor models: linear, ridge, LASSO, elastic net, random forest, histogram gradient boosting, support vector, extra trees, k-NN, and AdaBoost.

Figure 1: Top: Nonlinear setting (NLIN), Bottom: Nonadditive setting (NADD). Box plots of observational, interventional, and counterfactual queries of four different SCMs over 10 random initializations of the model and training data.

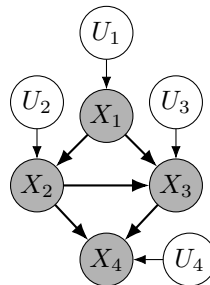




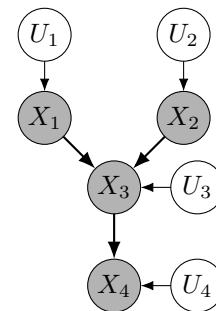
(a) Chain graph.



(b) Triangle graph.



(c) Diamond graph.



(d) Y graph.

Figure 2: Causal graphs used in our experiments.